Chemical Science

ROYAL SOCIETY OF CHEMISTRY

EDGE ARTICLE

View Article Online
View Journal | View Issue

Cite this: *Chem. Sci.*, 2024, **15**, 19534

All publication charges for this article have been paid for by the Royal Society of Chemistry

Regioselectivity switches between anthraquinone precursor fissions involved in bioactive xanthone biosynthesis†‡

Xiao Jing Lv,§[a] Chun Zhi Ai,§[b] Li Rong Zhang,[a] Xiu Xiu Ma,[c] Juan Juan Zhang,[d] Jia Peng Zhu[c] and Ren Xiang Tan *[ad]

Xanthone-based polyketides with complex molecular frameworks and potent bioactivities distribute and function in different biological kingdoms, yet their biosynthesis remains under-investigated. In particular, nothing is known regarding how to switch between the C_{4a}–C_{10} (C_{4a}-selective) and C_{10a}–C_{10} bond (C_{10a}-selective) cleavages of anthraquinone intermediates involved in biosynthesizing strikingly different frameworks of xanthones and their siblings. Enabled by our characterization of antiosteoporotic brunneoxanthones, a subfamily of polyketides from *Aspergillus brunneoviolaceus* FB-2, we present herein the brunneoxanthone biosynthetic gene cluster and the C_{10a}-selective cleavage of anthraquinone (chrysophanol) hydroquinone leading ultimately to the bioactive brunneoxanthones under the catalysis of BruN (an undescribed atypical non-heme iron dioxygenase) in collaboration with BruM as a new oxidoreductase that reduces the anthraquinone into its hydroquinone using NADPH as a cofactor. The insights into the driving force that determines whether the C_{10a}- or C_{4a}-selective cleavages of anthraquinone hydroquinones take place were achieved by a combination of multiprotein sequence alignment, directed protein evolution, theoretical simulation, chemical capture of hydroquinone tautomer, ^{18}O chasing, and X-ray crystal structure of the $BruN^{N441M}$ mutant, eventually allowing for the protocol establishment for the on-demand switch between the two ways of anthraquinone openings. Collectively, the work paves the way for the synthetic biology-based regeneration of uniquely structured high-value xanthones present in low abundance in complex mixtures, and helps to deepen the understanding on why and how such xanthones and their congeners are biosynthesized by different (micro)organisms in nature.

Received 20th September 2024
Accepted 4th November 2024

DOI: 10.1039/d4sc06369d

rsc.li/chemical-science

Introduction

Xanthone-based compounds form and function in different biological kingdoms, and constitute a unique family of natural products characterized by diverse molecular frameworks and various biological activities.[1–3] On one hand, the xanthone tricyclic scaffold facilitates the interaction of these molecules with diverse biological targets to display an array of important effects (*e.g.*, anti-cancer, neuroprotective, antimicrobial, anti-inflammatory, antiosteoarthritic, antimalarial, and anti-cardiovascular disease).[4,5] On the other hand, the type and position of substituent(s) anchoring on the tricyclic nucleus substantially or decisively influence their ultimate efficacy.[6,7] The natural xanthones are biosynthesized roughly in a life domain-dependent manner,[1–3] but the substitution patterns of the tricyclic system are largely inherited from precursors such as anthraquinones in fungi.[3] However, the mechanism underlying the downstream reaction steps of such precursors remains neglected or overlooked.

Distinct from plants[1] and bacteria,[2] fungi seem to be a richer source of xanthones with intriguing structures and potent bioactivities, as exemplified by brunneoxanthone E,[8] shamixanthone,[9,10] blennolide A,[11] secalonic acid A,[12] neosartorin,[13] beticolin 1,[14] geodin,[15,16] and trypacidin[17] (Fig. 1). As showcased in Fig. 1, most of the fungal xanthones and their oligomers are biosynthetically mediated by the ring fission of anthraquinone

[a]*State Key Laboratory Cultivation Base for TCM Quality and Efficacy, School of Pharmacy, Nanjing University of Chinese Medicine, Nanjing 210023, China. E-mail: rxtan@nju.edu.cn*

[b]*State Key Laboratory for Chemistry and Molecular Engineering of Medicinal Resources, Key Laboratory for Chemistry and Molecular Engineering of Medicinal Resources (Ministry of Education of China), Collaborative Innovation Center for Guangxi Ethnic Medicine, School of Chemistry and Pharmaceutical Sciences, Guangxi Normal University, Guilin 541004, China*

[c]*School of Medicine and Holistic Integrative Medicine, Nanjing University of Chinese Medicine, Nanjing 210023, China*

[d]*State Key Laboratory of Pharmaceutical Biotechnology, Institute of Functional Biomolecules, School of Life Sciences, Nanjing University, Nanjing 210023, China*

† The crystal structure of $BruN^{N441M}$ has been deposited in the Protein Data Bank (PDB), https://www.rcsb.org, with accession number 8YXS.

‡ Electronic supplementary information (ESI) available. See DOI: https://doi.org/10.1039/d4sc06369d

§ Contributed equally to this work.

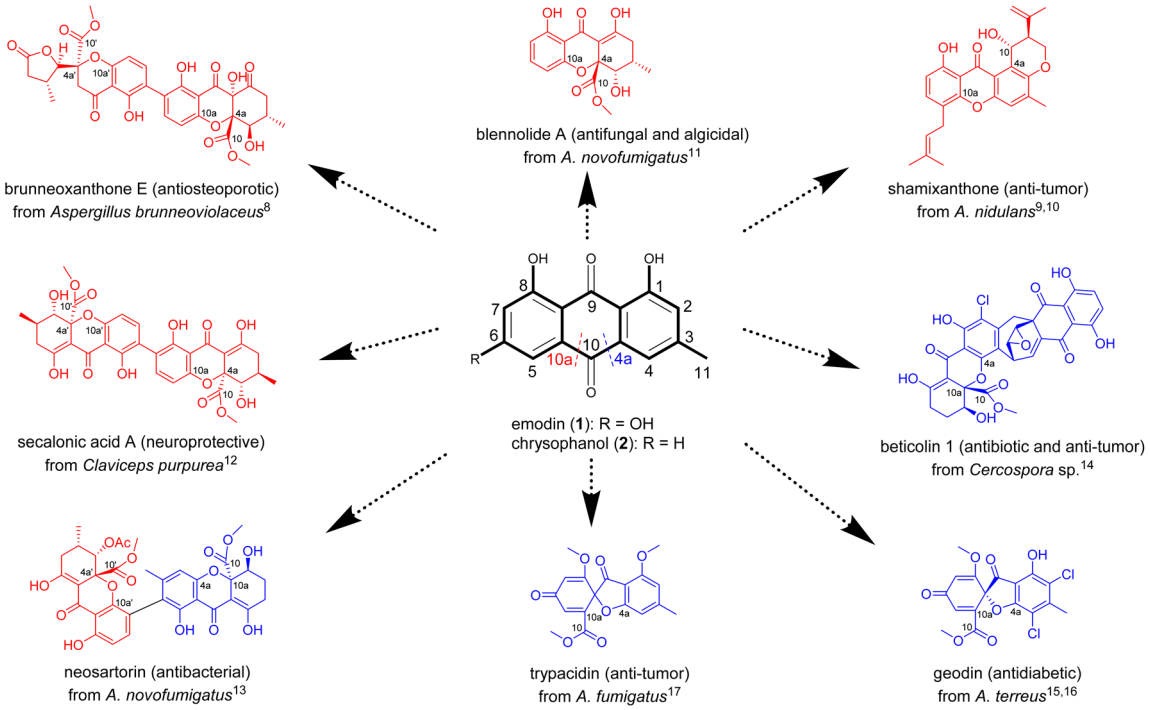

Fig. 1 A selection of bioactive fungal xanthones with the carbon skeleton formation depending biosynthetically on the C_{4a}–C_{10} (C_{4a}-selective, in blue) or C_{10a}–C_{10} (C_{10a}-selective, in red) bond cleavages of anthraquinone intermediates such as emodin (**1**) and chrysophanol (**2**).

intermediates such as emodin (**1**) and chrysophanol (**2**).[3] This has been repetitiously substantiated by the fast-evolving sequencing technologies and genome assembling approaches, which collectively enabled the identification of some unexpected biosynthetic gene clusters encoding anthraquinones and anthraquinone-derived xanthones.[3] Interestingly, the C_{4a}–C_{10} (C_{4a}-selective) and C_{10a}–C_{10} bond (C_{10a}-selective) cleavages of anthraquinone intermediates lead to distinct xanthone molecules with different bioactivities (Fig. 1). Accordingly, the C_{4a}- or C_{10a}-regioselectivities in the anthraquinone precursor cleavages as well as their switchability are of paramount importance for the *de novo* regeneration of substitution-oriented xanthones desirable for the drug discovery pipeline.

The C_{4a}- and C_{10a}-selective fissions of anthraquinones for the xanthone-related polyketide biosynthesis were believed to be catalyzed by Baeyer–Villiger monooxygenases (BVMO).[3] However, this was disproved by recent insights into the ring openings of anthraquinone precursors. In 2021, Lu *et al.* unraveled the two-enzyme (GedF and GedK) catalyzed C_{4a}-selective anthraquinone (questin) fission; or more specifically, in the presence of NADPH, GedF promotes the reduction of questin into its hydroquinone, which is subsequently accepted as substrate by GedK (an atypical cofactor-free dioxygenase) and eventually oxidized into desmethylsulochrin.[18] A year later, Rao and his co-workers reported the C_{4a}-selective cleavage of **2** in the chrysophanol hydroquinone (**3**) form by another enzyme pair consisting of a non-heme iron dioxygenase (BTG13) and a reductase (BTG7, also using NADPH as an electron donor).[14] In both cases, no oxidation happened upon the direct exposure of anthraquinones to GedK or BTG13, which became catalytically active after addition of sodium dithionite ($Na_2S_2O_4$) into the reaction media. The findings reinforced that GedK and BTG13 do not interact "effectively" with the anthraquinone molecules, but rather recognize as substrates the corresponding hydroquinones forming from the two-electron reduction of anthraquinones.[14,18,19] Another oxygenase (NsrF) was evidenced to catalyze the unselective cleavage of **2** to form diversely modified xanthones as a result of simultaneous fissions of C_{4a}–C_{10} and C_{10a}–C_{10} bonds of the same anthraquinone precursor.[13] We envisioned, and wished to experimentally prove, the interchangeability between the C_{4a}- and C_{10a}-selective fissions of anthraquinones; and if proven true, we were more curious about how to steer the trajectory of such cleavage reactions hopefully in an on-demand manner.

The reports describing the C_{4a}-selective[14,19] and unselective[13] anthraquinone fissions tempted us to search for an enzyme counterpart that catalyzes the C_{10a}-selective cleavage of such quinone precursors. Catching our eyes was *Aspergillus brunneoviolaceus* FB-2 (*A. brunneoviolaceus*) which produces various xanthone dimers including brunneoxanthone E with an antiosteoporotic activity (Fig. 1).[8] In particular, brunneoxanthone E and its siblings (brunneoxanthones A–D and penibishexahydroxanthone A) belong to the 2,2′-linked dimers with all tailored xanthone monomers derived from monodictyphenone (**4a**) rationalized to form from the C_{10a}-selective cleavage of **2**.[8] With our confidence in the fungal (*A. brunneoviolaceus*) enzyme that catalyzes the C_{10a}-selective cleavage, we performed the present investigation to identify the brunneoxanthone biosynthetic gene (shortened as "*bru*") cluster through a combination of genome sequencing, multiprotein sequence alignment, gene

inactivation, and heterologous expression. From the *bru* cluster, BruMN were evidenced to play catalytic roles in the C_{10a}-selective fission of **2** into **4a**. Starting from the enzyme, we established the first protocol for freely operational switches between the C_{4a}- and C_{10a}-selective cleavages of **2**, the common anthraquinone precursor of diverse xanthones and their oligomer in nature.[1–3,8] Taken together, the work offers a versatile foundation for the synthetic biology-based access to high-value xanthones and their congeners existing as (very) minor components in complex mixtures, and helps to understand why and how xanthones and their variants are, or must be, produced in different (micro)organisms.

Results and discussion

BruMN mediate the C_{10a}-selective cleavage of chrysophanol

The brunneoxanthone structures[8] suggested that the C_{10a}-selective fission of chrysophanol (**2**) was most likely a key step for constructing these highly tailored xanthone dimers in *A. brunneoviolaceus*. This motivated us to identify the gene cluster for biosynthesizing brunneoxanthone E from the fungal genome which was sequenced and subsequently analyzed using antiSMASH (antibiotics and secondary metabolite analysis shell) (fungal version).[20] The attempt identified a total of 26 polyketide synthase (PKS)-containing biosynthetic gene clusters (Fig. S1‡), of which six were predicted to express non-reducing PKSs (NR-PKSs). Typical of containing an NR-PKS gene, the *bru* cluster was proposed to encode likely the brunneoxanthone E biosynthesis (Fig. 2A and Table S1‡) from our sequence alignment with the *nsr*, *agn*, *sec* and *dmx* clusters, which are responsible for the biosynthesis of neosartorin in *A. novofumigatus*,[13] agnestins in *Paecilomyces variotii*,[21] secalonic acids in *Claviceps purpurea*,[11,12] and cryptosporioptides in *Cryptosporiopsis* sp,[22] respectively (Table S2 and Fig. S2‡). Next, we sought out to confirm the proposal through the gene inactivation strategy as described.[23] The individual gene function in the *bru* cluster (Fig. 2A and Table S2‡) was annotated to be similar to those in the *nsr* cluster from *A. novofumigatus*.[13] This agreed with the structural comparability between the xanthone monomers produced by the two *Aspergillus* species.[8,13] In particular, the *bruN* gene in the *bru* cluster was annotated to encode an oxygenase with a 47% sequence identity to NsrF assumed to be an oxygenase involved in sculpting **2** into the xanthone monomers leading to neosartorin.[13] We therefore deleted the *bruN* gene from the *bru* cluster to obtain the Δ*bruN* mutant. As indicated by the liquid chromatography-mass spectrometry (LC-MS) analysis, **2** was abundant in the Δ*bruN* culture but undetectable in that of the wild-type (WT) strain (Fig. 2C and S3‡).[8] Owing to the deprival of the BruN-catalyzed oxidative cleavage, the Δ*bruN* strain did not produce brunneoxanthone E, which remained detectable in the WT culture (Fig. 2C and S3‡). The observation pinpointed that the *bru* cluster governed the brunneoxanthone biosynthesis with BruN catalyzing the C_{10a}-selective cleavage of **2** (Fig. 2B). The assumption agreed with the predicted function of the **2**-expressing six-gene set (*bruHIJKMO*), encoding respectively a short chain dehydrogenase (BruH), a thioesterase (BruI), an NR-PKS (BruJ), a dehydratase (BruK), an oxidoreductase (BruM), and a decarboxylase (BruO). Particularly noteworthy was that these enzymes displayed a 52%∼89% amino acid (AA) sequence identity to the counterparts that sculpted **2** into diverse xanthone derivatives (Table S2‡), such as neosartorin,[13] agnestins,[21] secalonic acids,[12] and cryptosporioptides.[22]

As reported,[14,18] the ring opening of **2** could be accomplished by an enzyme pair consisting of a reductase and a dioxygenase. Our attention was therefore focused on BruM, the only oxidoreductase in the *bru* cluster. BruM was shown homologous both to NsrR (58%) that catalyzes the emodin (**1**) reduction to mediate the neosartorin (xanthone dimer) biosynthesis,[13] and to BTG7 (51%) involved in the **2** reduction to facilitate the construction of beticolin 1, a xanthone–anthraquinone hybrid.[14] To confirm their partnership, we generated the AO-*bruM* and AO-*bruN* transformants as well as the AO-*bruMN* co-transformant using *A. oryzae* NSAR1 strain (shortened as "AO" hereafter), a quadruple auxotrophic mutant strain (*niaD*$^-$, *sC*$^-$, Δ*argB*, *adeA*$^-$) applicable for the biosynthetic studies on fungal natural products.[23,24] With that, **2** was supplemented separately in the cultures of the three transformants. The results showed that the AO-*bruMN* co-transformant produced a major product identified as **4a** (Fig. 2D(iv))[25] by its MS and ^{1}H and ^{13}C NMR data (Table S5 and Fig. S24–S26‡). However, the AO-*bruN* transformant generated as well a lower abundance of **4a** (Fig. 2D(iii)) presumably owing to an unknown AO-expressed reductase similar to our earlier observation.[26] Furthermore, AO-*bruM* transformant and AO yielded a common byproduct identified as emodinic acid (Fig. 2D(i) and (ii)) by comparing its MS and ^{1}H NMR data with those reported (Table S9, Fig. S34 and S35‡).[23] Emodinic acid forms from emodin (**1**) *via* the C_9–C_{9a} cleavage catalysed by an AO-produced BVMO.[23] Our characterization of emodinic acid from the **2**-exposed culture signified the presence of another AO oxidase that catalyzed the 6-hydroxylation of **2** (ahead of C_9–C_{9a} cleavage) or 6-deshydroxy emodinic acid (after the C_9–C_{9a} cleavage of **2**). Such lines of evidences underpinned that the BruMN enzyme pair plays a decisive role in the C_{10a}-selective fission of **2** to facilitate the brunneoxanthone biosynthesis.

Regioselectivity and substrate promiscuity of BruN

To get more insights into the catalytic property of BruN, the codon-optimized *N*-terminally His-tagged BruN was cloned into the pET28a vector and overexpressed in *E. coli* BL21 (DE3) with the obtained yellow enzyme protein purified by an Ni-NTA affinity chromatography (Fig. S4‡). As predicted, no activity was appreciable when **2** was incubated with purified BruN in the (co-)presence of cofactors including NADPH, NADH, FAD, and FMN (Fig. S5A‡). However, upon its co-exposure to BruN and $Na_2S_2O_4$, **2** was oxidized into **4a**, but not cephalanone F (**4b**) as a C_{4a}-selectively cleaved product of **2** under the BTG7/BTG13 catalysis (Fig. S5A‡).[14] This experimentation confirmed that BruN did not directly accept **2** as substrate although bioinformatically predicted to be a BVMO that might catalyze the C_{4a}- or C_{10a}-selective cleavage of anthraquinones. To reinforce its catalyst partnership with BruN, BruM was heterologously

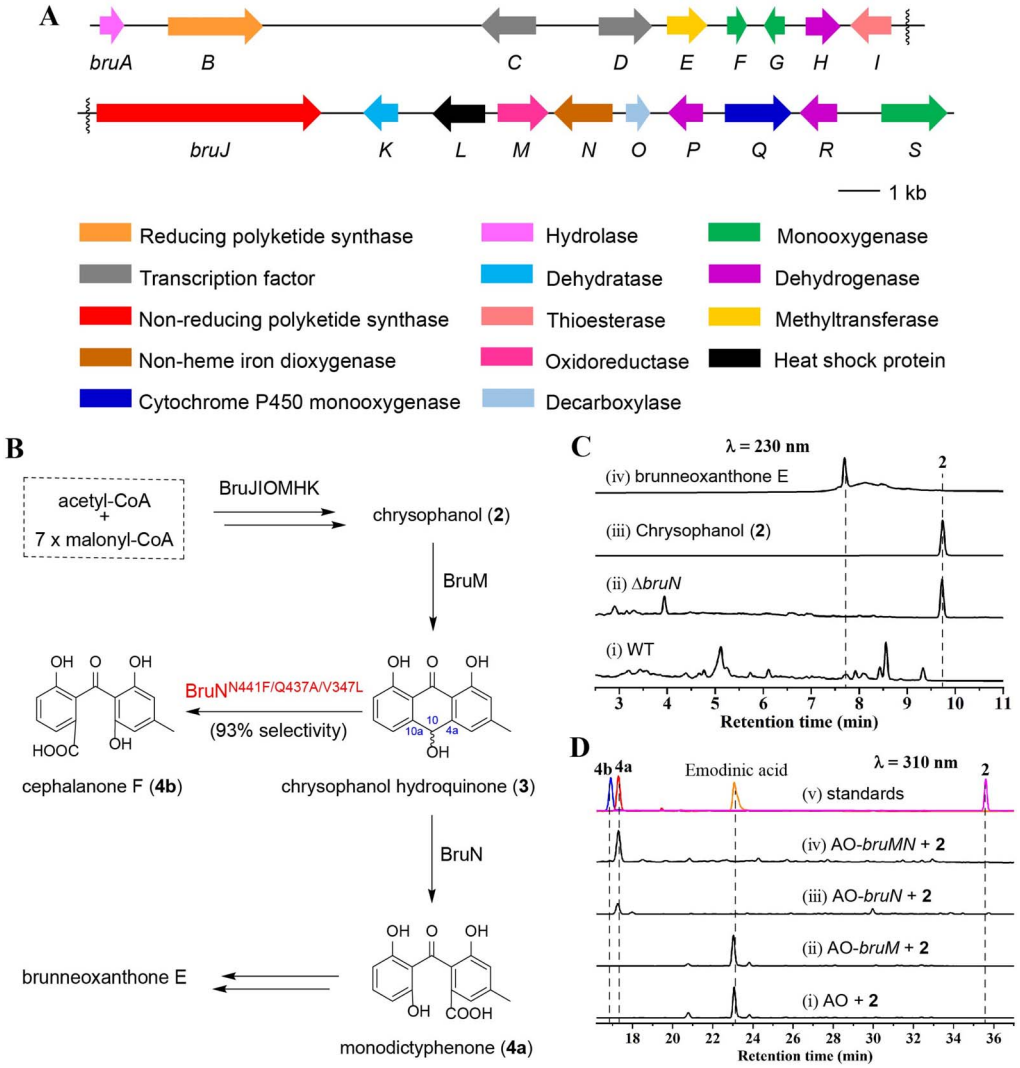

Fig. 2 Identification of BruMN cleaving C_{10a}-selectively chrysophanol (**2**) from the brunneoxanthone E biosynthetic gene (*bru*) cluster in the *A. brunneoviolaceus* genome. (A) Predicted functions of enzymes in the *bru* cluster. (B) The brunneoxanthone E biosynthesis is mediated by the BruN catalyzed C_{10a}-selective cleavage of chrysophanol hydroquinone (**3**) into monodictyphenone (**4a**). The BruN$^{N441F/Q437A/V347L}$ mutant found herein catalyzed the C_{4a}-selective cleavage of **3** into cephalanone F (**4b**) with a 93% C_{4a}-selectivity. (C) The *bruN* deletion led to the **2** boost. The EtOAc extracts from the cultures of the Δ*bruN* and wild-type (WT) strains of *A. brunneoviolaceus* were analyzed by LC-MS using an acetonitrile/water gradient (30 : 70 → 100 : 0, within 13 min). (D) BruN accepts **3**, rather than **2**, as substrate that was C_{10a}-selectively cleaved into **4a**. The *bruMN*, *bruM*, and *bruN* genes were expressed in *A. oryzae* (AO) followed by exposure to **2**, indicating that the AO-*bruMN* co-transformant allowed for the **4a** production. The LC-MS analysis was performed using the duration-dependent methanol/water (containing 0.1% formic acid) gradients (0 → 10 min, 5 : 95 → 35 : 65; 10 → 35 min, 35 : 65 → 100 : 0; 35 → 40 min, pure methanol).

expressed and purified as was done for the pure BruN protein (Fig. S4‡). In the presence of NADPH (2 mM), **2** (250 μM) was incubated with an equimolar (15 μM) mixture of BruM and BruN, leading ultimately to the production of **4a** as indicated by our LC-MS analysis of the obtained reaction mixture (Fig. S5A‡). Despite its lower abundance, **3** was detected in the extracted ion chromatogram of the enzymatic reaction mixture resulting from the first 2 minutes exposure of **2** to BruM and NADPH, but became undetectable after reacted for 10 minutes (Fig. S5B‡), thus highlighting that **3** is fairly labile and tends to be re-oxidized into **2** in air.[14] The attempt failed to identify the formation of **4b**, thereby establishing the BruN's C_{10a}-selectivity which is independent of BruM (Fig. 2B and S5‡). To test its substrate promiscuity, the equimolar mixture of BruM and BruN was exposed to each of chrysophanol analogs (available in our laboratory) in the presence of NADPH, followed by the LC-MS analysis of resultant products (Fig. S6‡). Unexpectedly, aloe emodin (**5**) was shown to be the most favorable substrate (Fig. S7‡). Also cleaved by the enzyme pair were **2**, rhein (**7**), emodin (**1**), and physcion (**6**) with the transformation rates around 58%, 32%, 5%, and 2%, respectively (Fig. S6 and S7‡). However, no reaction was discerned after the two enzymes were co-exposed to emodin 8-*O*-β-D-glucopyranoside (**8**) (Fig. S7‡). To ascertain the regioselectivity in the ring opening, we scaled up the BruMN catalyzed reaction of **1** and **5–7**, leading ultimately to the identification of 11-hydroxylated monodictyphenone (**5a**),

a C_{10a}-selective fission product from **5** (Table S7, Fig. S29, and S30‡). Although detected by the LC-MS analysis (Fig. S6‡), the cleaved products from other test compounds failed to be purified in sufficient quantities for the NMR measurement, presumably because of their (much) lower reaction rate in exposure to the enzyme pair (*vide supra*). Collectively, this set of experimentations reinforced the C_{10a}-selectivity and a broader substrate scope of BruN in cleaving **2** and its analogs.

Regioselectivity reversal of BruN and BTG13 by directed protein evolution

From a biochemical viewpoint,[27] the enzyme catalysis is usually accomplished through (i) self-adjusting conformation to accept substrate, (ii) distorting or directing the substrate to follow a specific mechanism, and (iii) re-positioning its key AA residues to create a particular microenvironment to allow the reaction to proceed efficiently. In most or all cases, the reaction selectivity depends largely on several residues in the enzyme molecule, which are spatially close enough to the catalytic center. This dogma gave us an impetus to reverse the C_{10a}-selectivity of BruN in opening anthraquinone ring of **2** through the directed protein evolution, which was proved effective in changing the catalytic trajectory of ChaP, a bacterial dioxygenase.[28] To validate or generalize the strategy, BTG13 was chosen and processed in parallel owing to its oppositely selective (C_{4a}–C_{10} bond) fission of **2** and crystal structure availability.[14]

To minimize randomness, we aligned the sequences of all enzymes reported to catalyze the C_{10a}- and C_{4a}-selective cleavages of anthraquinones (Fig. S8‡). Thanks to the AlphaFold3 program,[29] such multi-protein sequence alignments facilitated our prediction of the three-dimensional (3D) BruN structure, which was comparable to the crystal structures of its single-site mutant ($BruN^{N441M}$) and BTG13 (Fig. S9‡).[14] But our mutagenesis efforts were further frustrated by too many "selectivity-related" AA residues of the C_{10a}- or C_{4a}-cleaving enzymes that nested in different phylogenetic clades (Fig. 3A and S8‡). Docking between BruN and chrysophanol hydroquinone (**3**) was therefore conducted to suggest the selectivity-sensitive (closer than 5 Å from **3**) AA residues (Fig. 3B), such as F55, R58, I91, A164, F243, G244, N245, K246, M247, V347, T435, D436, Q437, V440, N441, F442, and R452 (Fig. 3C). These "sensitive residues" contributing (most) likely to the C_{10a}-selectivity of BruN were mutated individually to the AA residues appearing (more) frequently in the C_{4a}-selective enzyme counterparts. All BruN variants obtained were heterologously expressed and purified as *N*-terminally His-tagged proteins as done for BruN (Fig. S10‡), followed by the catalysis assessment by being incubated at 30 °C for 2 h in the co-presence of BruM (15 μM), **2** (250 μM), and NADPH (2 mM). Particular attention was paid to the product detection by the LC-MS analysis to roughly quantify the amounts of **4a** and **4b** resulting from, and thus adopted as indicators of, the C_{10a}- and C_{4a}-selective fissions of **2**, respectively. Notably, two BruN variants ($BruN^{N441M}$ and $BruN^{N441W}$) exhibited substantially reversed regioselectivity as reflected by their catalysis for the conversion of **2** into **4b** as a product with the **4a**/**4b** ratio around 77 : 23 ($BruN^{N441M}$) and 70 : 30 ($BruN^{N441W}$), respectively. Other variants (*e.g.*, $BruN^{F243G}$, $BruN^{G244P}$, $BruN^{N245V}$, $BruN^{D436P}$, $BruN^{V440I}$, and $BruN^{F442G}$) were also generated but their **4a**/**4b** ratios were found higher than 90 : 10 (Fig. 4 and S11‡). Unfortunately, such single-site mutations of BruN failed to afford any mutant capable of catalyzing the purely C_{4a}-selective fission of **2** as does BTG13.[14] Such a partially negative consequence was counteracted by our identification of two BTG13 mutants, $BTG13^{M427N}$ and $BTG13^{M427V}$, both catalyzing a 100% conversion of **2** into **4a** in a regioselective manner entirely different from intact BTG13 that allowed the **4b** formation only.[14] In other words, the findings strengthened our confidence in reversing BruN's regioselectivity *via* the directed protein evolution, although other single-site BTG13 mutants (*e.g.*, $BTG13^{M427F}$ and $BTG13^{M427P}$) were shown catalytically identical to BTG13 (Fig. 4, S12, and S13‡). As signified by the $BruN^{N441M}$ and $BruN^{N441W}$ catalysis (*vide supra*), the N441 mutation for BruN was most likely substantial or essential for its reversal to the C_{4a}-selectivity, but not necessarily mutated to Met and Trp despite their frequent presence in the C_{4a}-selectively cleaving enzymes (Fig. 3C). This encouraged us to perform the saturation mutagenesis[28,30,31] by mutating N441 to each of the rest 17 protein AAs (Fig. S10‡). As a step forward, the $BruN^{N441F}$ mutant displayed an improved regioselectivity reversal (Fig. 4 and S14‡).

In pursuing the highly regioselective BruN variant(s), the relatively effective single-site mutants, $BruN^{N441F}$, or $BruN^{N441M}$, or $BruN^{N441W}$ were subjected to our double mutation efforts. Thus, the rest 16 AA residues that predicted to be "selectivity-sensitive" (Fig. 3C) were individually changed into the counterparts of C_{4a}-selective enzymes (Fig. 3C) and others if perceived necessary (Fig. S10‡). Interestingly, the abundance of **4b** was found escalated in the reaction solution of **2** under the $BruN^{N441W/R452V}$ catalysis with the **4a**/**4b** ratio approaching 39 : 61, although poor regioselectivity reversal was discerned with other double-site mutants, such as $BruN^{N441M/R452V}$, $BruN^{N441W/R58V}$, $BruN^{N441W/N245V}$, and $BruN^{N441W/V347A}$ (Fig. 4 and S15‡). Moreover, starting from the N441-to-Phe mutant, we obtained several double-site variants like $BruN^{N441F/Q437A}$, $BruN^{N441F/V440I}$, $BruN^{N441F/V347L}$, $BruN^{N441F/Q437P}$, $BruN^{N441F/A164L}$, $BruN^{N441F/Q437G}$, and $BruN^{N441F/Q437M}$, all exhibiting improved yields of **4b** in the same catalysis assay (Fig. 4 and S16‡).

To obtain more efficient mutants, we were motivated to generate multi-site BruN mutants from the promising variants such as $BruN^{N441W/R452V}$, $BruN^{N441F/Q437A}$, and $BruN^{N441F/V440I}$. The subsequent catalysis assay showed that $BruN^{N441F/V440I/V347L}$ and $BruN^{N441F/Q437A/V347L}$ possessed the substantially improved regioselectivity reversals as reflected by the **4a**/**4b** ratios around 50 : 50 and 43 : 57 (Fig. 4, S16, and S17‡). Furthermore, during such repeated mutation attempts, we observed and thus envisioned that enzymatic reaction condition (RC) might play roles in reversing the regioselectivity. Thus, we re-evaluated the **4a**/**4b** ratio values after **2** was treated with the promising mutants (*vide supra*) at varied concentrations within differentiated reaction durations (Fig. 5A). Surprisingly, the higher (>90%) C_{4a}-selectivity was discerned with $BruN^{N441F/Q437A}$, $BruN^{N441F/V347L}$, $BruN^{N441F/Q437P}$, $BruN^{N441F/V440I/V347L}$, and $BruN^{N441F/Q437A/V347L}$ variants with the **4a**/**4b** ratios around

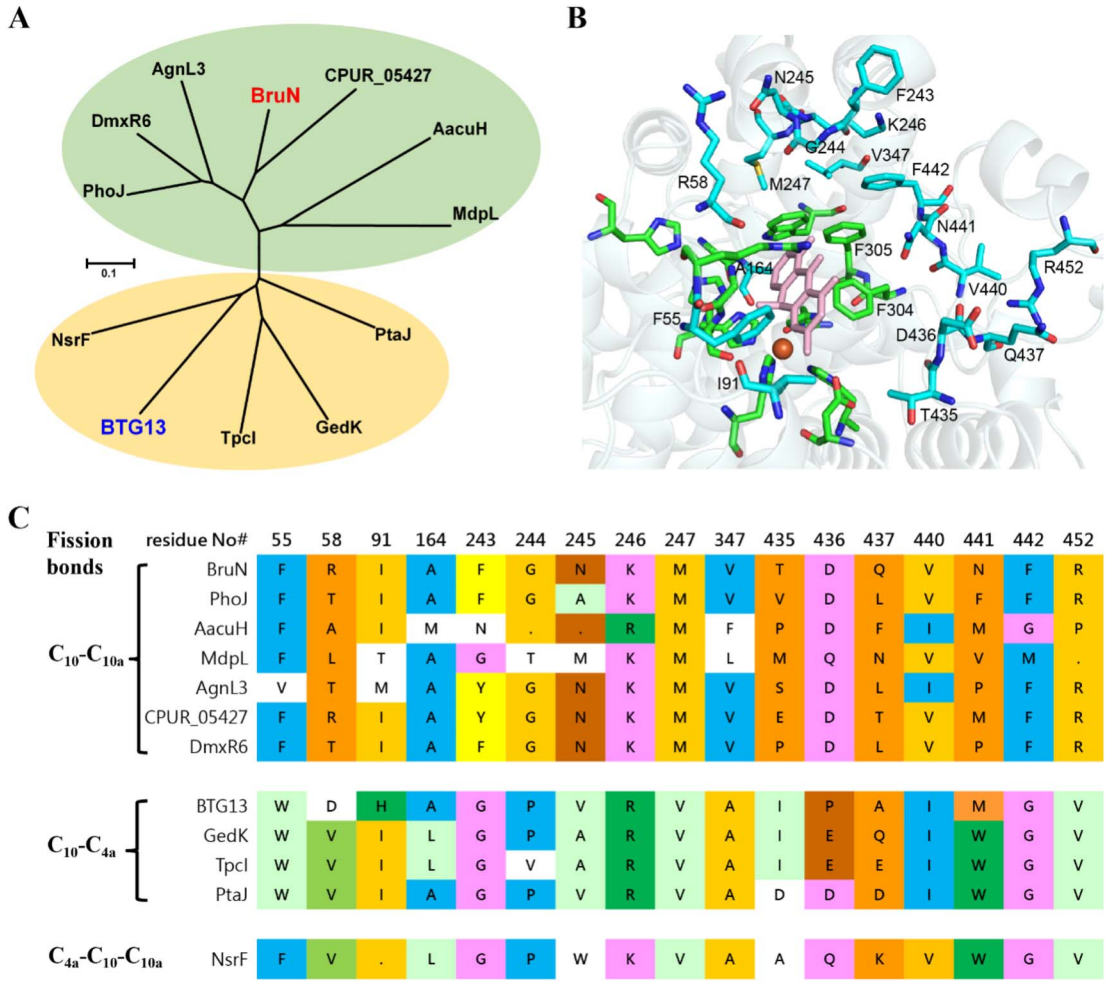

Fig. 3 Sequence alignment of BruN with reported homologues that cleave the C_{4a}–C_{10} and C_{10a}–C_{10} bonds of anthraquinones. (A) Nesting in strikingly different clades were BruN (this work) and BTG13,[14] which catalyze respectively C_{10a}- and C_{4a}-selective fissions of chrysophanol (**2**). (B) The docking of BruN (Alphafold3 modeled)[29] to chrysophanol hydroquinone (**3**) highlighted the conserved (green) and varied residues (cyan) that are ≤5 Å distant from the **3** molecule in collaboration with multi-protein sequence alignments. (C) Multi-protein sequence alignments suggested a total of 17 amino acid (AA) residues associated possibly with the regioselective fission of C_{4a}–C_{10} and C_{10a}–C_{10} bonds of anthraquinones.

10 : 90, 9 : 91, 9 : 91, 8 : 92, and 7 : 93, respectively (Fig. 2B, 5B and S18‡). Overall, the aforementioned findings realized the switch between the C_{4a}- and C_{10a}-selective fissions of chrysophanol (**2**) under the catalysis of BruN and BTG13.

Insights into the regioselectivity and interchangeability of BruN and BTG13 catalyses

To deepen our understanding on the regioselectivity in the enzymatic catalysis, we were motivated to obtain the BruN crystal by consulting the BTG13 crystallization protocol.[14] Unfortunately, it was unsuccessful. We therefore tried to get the crystal structure of BruN mutants generated for investigating the regioselectivity (*vide supra*). Fortunately, the $BruN^{N441M}$ crystal was afforded and determined at 3.6 Å resolution to resemble that of BTG13 (Table S10 and Fig. S9‡). As discerned with BTG13,[14] an iron ion at the crystal center coordinated with four histidines (H63, H166, H308, and H386), a carboxylated-lysine (kcx389), and a water molecule. The iron ion was ascertained by the divalent cation replacement[32] and the inductively coupled plasma mass spectrometry (ICP-MS) (Fig. S19‡). The AA residues around the iron center are conserved among the BruN homologs (Fig. S8‡) and were indispensable for BruN's catalytic activity as verified by our site-directed mutations (Fig. S20 and S21‡). Despite the same iron coordination mode, $BruN^{N441M}$ and BTG13 crystals showed different binding pockets above the iron cofactor (Fig. S9‡). This observation, along with the directed protein evolution experiments, prompted us to hypothesize that the shared substrate, chrysophanol hydroquinone (**3**), may exist in several or diverse tautomers (*e.g.*, **3a** and **3b**) in the BruN- or BTG13-created microenvironments; but only particularly structured tautomers could effectively interact with enzymes to form the regioselectively cleaved products from **3**. The assumption agreed with the keto–enol tautomerism of the anthraquinone hydroquinone intermediate involved in the aflatoxin B1 biosynthesis.[33] While re-oxidizable into **2** in exposure to air,[14,18,34] hydroquinone **3** tautomerizes rapidly, and the tautomers are too

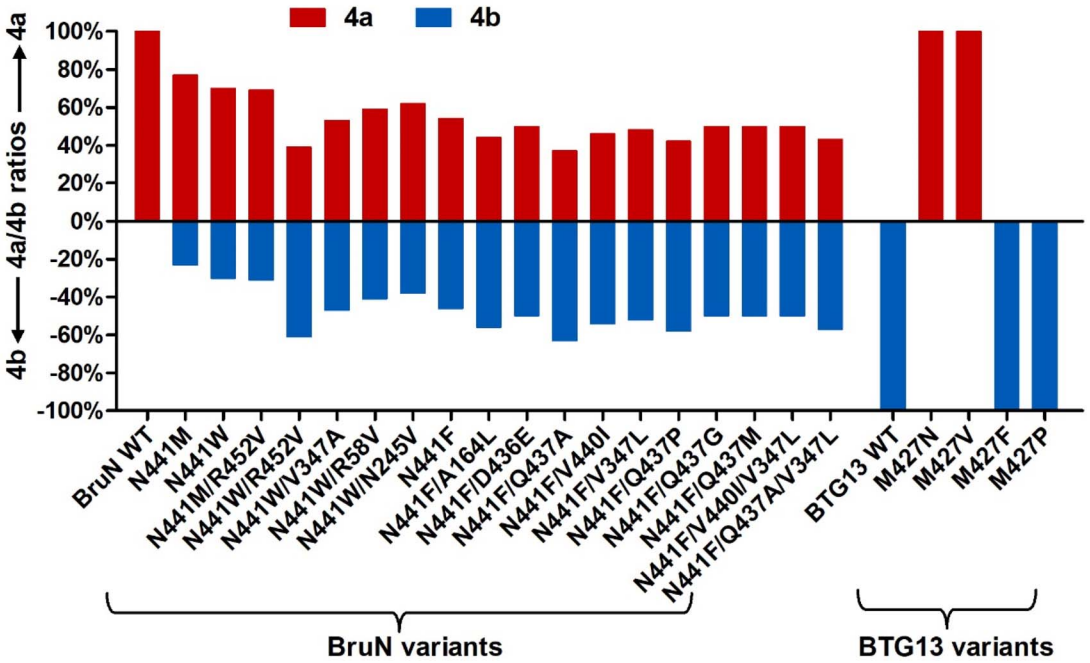

Fig. 4 Yield comparison between monodictyphenone (**4a**) and cephalanone F (**4b**) formed as the C_{10a}- and C_{4a}-selective fission products, respectively, from chrysophanol (**2**) under the catalysis of BruN variants (NVs) and BTG13 mutants in the presence of equimolar amount BruM (15 μM), substrate **2** (250 μM), and NADPH (2 mM, as a cofactor). The regioselectivity reversal assay was performed at 30 °C for 2 h. Depicted were the NVs' mutants displaying appreciable selectivity reversals signified by the **4b** formation (see Fig. 2B). The M427N and M427V mutants of BTG13, a C_{4a}-selective catalyst,[14] were demonstrated by the assay to catalyze the conversion of **2** into **4a** with a 100% C_{10a}-selectivity.

interchangeable to be captured individually. We were tempted to chemically confirm the tautomerism. Thus, chrysophanol (**2**) was methylated with Me_2SO_4 to obtain its methylated product, which was further reduced by $Na_2S_2O_4$ followed by immediate methylation with Me_2SO_4 once again to give mainly **12**, the permethylated derivative of **3** (Fig. S22‡), whose structure was proven identical to that defined earlier.[35] Such efforts verified the tautomerism of **3** since both **3a** and **3b** can be permethylated into **12**. Moreover, the isotope labeling experiment was performed using $^{18}O_2$, thereby confirming the dioxy catalytic mechanism of dioxygenase BruN rather than Baeyer–Villiger oxidation (Fig. S24‡). Accordingly, as illustrated in Scheme 1, the BruM/BTG7-catalyzed (two-electron) reduction of chrysophanol (**2**) gave chrysophanol hydroquinone (**3**) that tends to tautomerize into **3a** and **3b**, and probably others. In the presence of dioxygen, BruN interacts fruitfully with the tautomer **3a** with 10,10a-double bond involved in the catalytic complex **I**, but BTG13 prefers to act towards **3b** with 10,4a-double bond bound to the enzyme to form complex **I′**. Next complexes **I** and **I′** undergo the double bond cleavages to afford **4a** and **4b** presumably *via* intermediates **II–V** and **II′–V′**, respectively, as if carotenoids are converted into ketone and/or aldehyde products under the catalysis of carotenoid cleavage oxygenases with the iron cofactor coordinated with four His residues, too.[36]

The above proposal agreed with our theoretical simulations. The geometric optimization and relative energy were calculated at B3LYP level to suggest four lower-energy conformations (LECs) for each of **3a** and **3b** (see **3a1–3a4** and **3b1–3b4** in Fig. S23‡). All the eight LECs were individually docked to BruN, $BruN^{N441M}$, and BTG13. Interestingly, the average binding free energies ($\Delta G_{binding}$) of BruN to **3a** ($-25.32 \sim -23.42$ kJ mol^{-1}) are lower than that to **3b** ($-23.21 \sim -22.28$ kJ mol^{-1}). In contrast, the $\Delta G_{binding}$ value of BTG13 to **3a** ($-24.86 \sim -23.37$ kJ mol^{-1}) were higher than that to **3b** ($-27.34 \sim -23.74$ kJ mol^{-1}) (Table S11‡). More interestingly, molecular dioxygen was shown to be able to access the 10,10a-double bond of **3a3** interacted with BruN (Fig. 6A), and the 10,4a-double bond of **3b1** docked with BTG13 (Fig. 6B). In compliance with the mutation experiments (Fig. S21‡), we did detect the π–π stacking interactions of **3a** and **3b** with F304 (in BruN) and F292 (in BTG13), respectively, thereby confirming the previously reported important role of this phenylalanine residue in the enzymatic catalysis.[14]

Also important is BruN's N441 residue that hydrogen-bond with **3a** to drive the 10,10a-double bond closer to the catalytic site (Fig. 6A). However, such hydrogen-bonding interaction between **3a** and the N441 residue in BruN was deprived in the $BruN^{N441M}$ mutant (Fig. 6C and D), which was thus rendered "liberated" to form other optional binding conformations with both **3a3** (Fig. 6C) and **3b2** (Fig. 6D). Agreeing with the experimental observation (Fig. 4), dioxygen was accessible when $BruN^{N441M}$ interacted with **3a3** (Fig. 6C) and **3b2** (Fig. 6D) to drive respectively the 10,10a- and 10,4a-double bonds closer to the catalytic center. This observation explained at least in part why both **4a** and **4b** were produced from the $BruN^{N441M}$ catalyzed fission of **3** that was cleaved in its tautomer forms **3a** and

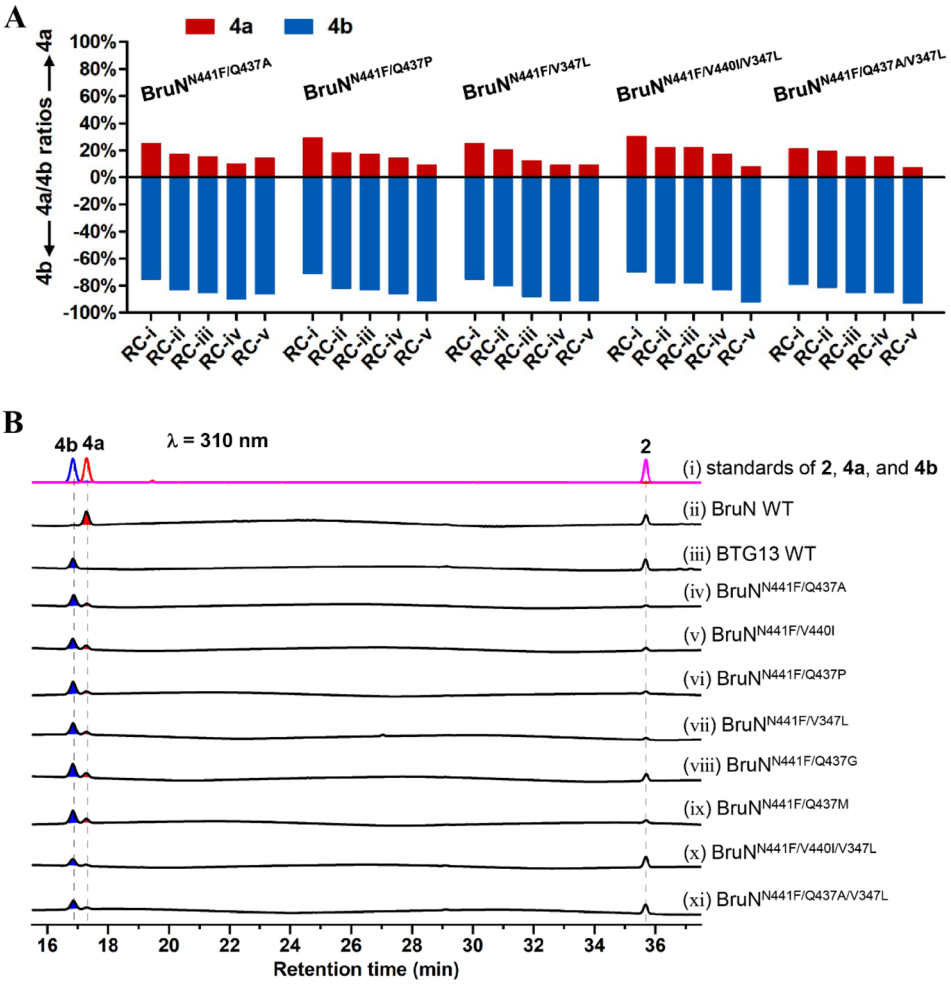

Fig. 5 Reaction condition (RC) optimization for multiply muted BruN variants (NVs). (A) Reaction duration and protein concentration were optimized at 30 °C for the NVs capable of catalyzing the cleavage of chrysophanol (**2**) into cephalanone F (**4b**) with a substantial (>70%) C_{4a}-selectivity in the presence of BruM and NADPH as specified below: (RC-(i)) 60 μM NVs, 25 μM BruM, 4 mM NADPH, 1 hour; (RC-(ii)) 80 μM NVs, 40 μM BruM, 4 mM NADPH, 30 min; (RC-(iii)) 100 μM NVs, 100 μM BruM, 5 mM NADPH, 15 min; (RC-(iv) and RC-(v)) 120 μM NVs, 120 μM BruM, 6 mM NADPH, 10 min. Substrate **2** was either 250 (from RC-(i) through RC-(iv)) or 125 μM (RC-(v)). (B) HPLC profiling for monodictyphenone (**4a**) and (**4b**) generating from **2** under the NVs' catalysis. The triple mutant ($BruN^{N441F/Q437A/V347L}$) exhibited the highest (93%) C_{4a}-selectivity. The C_{10a}- and C_{4a}-selective fission products, **4a** and **4b**, were quantified by the LC-MS analysis (Fig. S18‡).

3b, respectively. Moreover, the binding energies of $BruN^{N441M}$ with **3a** was lower than that with **3b** (Table S11‡) agreed roughly with the **4a**/**4b** ratio around 77 : 23. Collectively, our experimentation and computation corroborated the C_{10a}- and C_{4a}-selectivity and interchangeability of BruN and BTG13 in catalyzing the ring-openings of chrysophanol (**2**) after the two-electron reduction into chrysophanol hydroquinone (**3**).

The C_{4a}- and C_{10}-selective cleavage of anthraquinones is widely involved in the fungal biosynthesis of structurally diverse bioactive xanthones as enumerated in Fig. 1. But the bond fission mechanism was misunderstood to be results of the Baeyer–Villiger oxidation reaction before Lu's and Rao's groups recognized the two-electron reduction of anthraquinone substrates into the corresponding hydroquinone forms as a prerequisite for such ring openings.[14,18] As additional insights into the topic, this work unravels the tunability between the C_{10a}- and C_{4a}-selectivities in cleaving **2** after its reduction into **3** by deepening the understanding on the catalytic features of BruN and BTG13 through directed protein evolution, chemical capture of chrysophanol hydroquinone tautomers (*e.g.*, **3a** and **3b**), ^{18}O chasing experiment, theoretical simulations starting from the structures of BruN (AlphaFold3 modeled),[29] $BruN^{N441M}$, and BTG13.[14] According to our experimental results, the N441 site in BruN corresponding to M427 site in BTG13 is essential for the reversal between C_{10a}- and C_{4a}-selectivity. For BruN, polar AA (N441) was mutated to non-polar aromatic amino acid phenylalanine ($BruN^{N441F}$) to facilitate the C_{10a}-to-C_{4a} selectivity switch, which could be further improved by simultaneous double or multiple mutation of its neighboring AAs (*e.g.*, V347L, T435–F442), as evidenced from the superior catalytic performance of $BruN^{N441F/Q437P}$, $BruN^{N441F/V440I/V347L}$, and $BruN^{N441F/Q437A/V347L}$. The observation could be rationalized by the mutation-reshaped binding cavity that favored the binding of **3b** tautomer with the mutants such as $BruN^{N441M}$

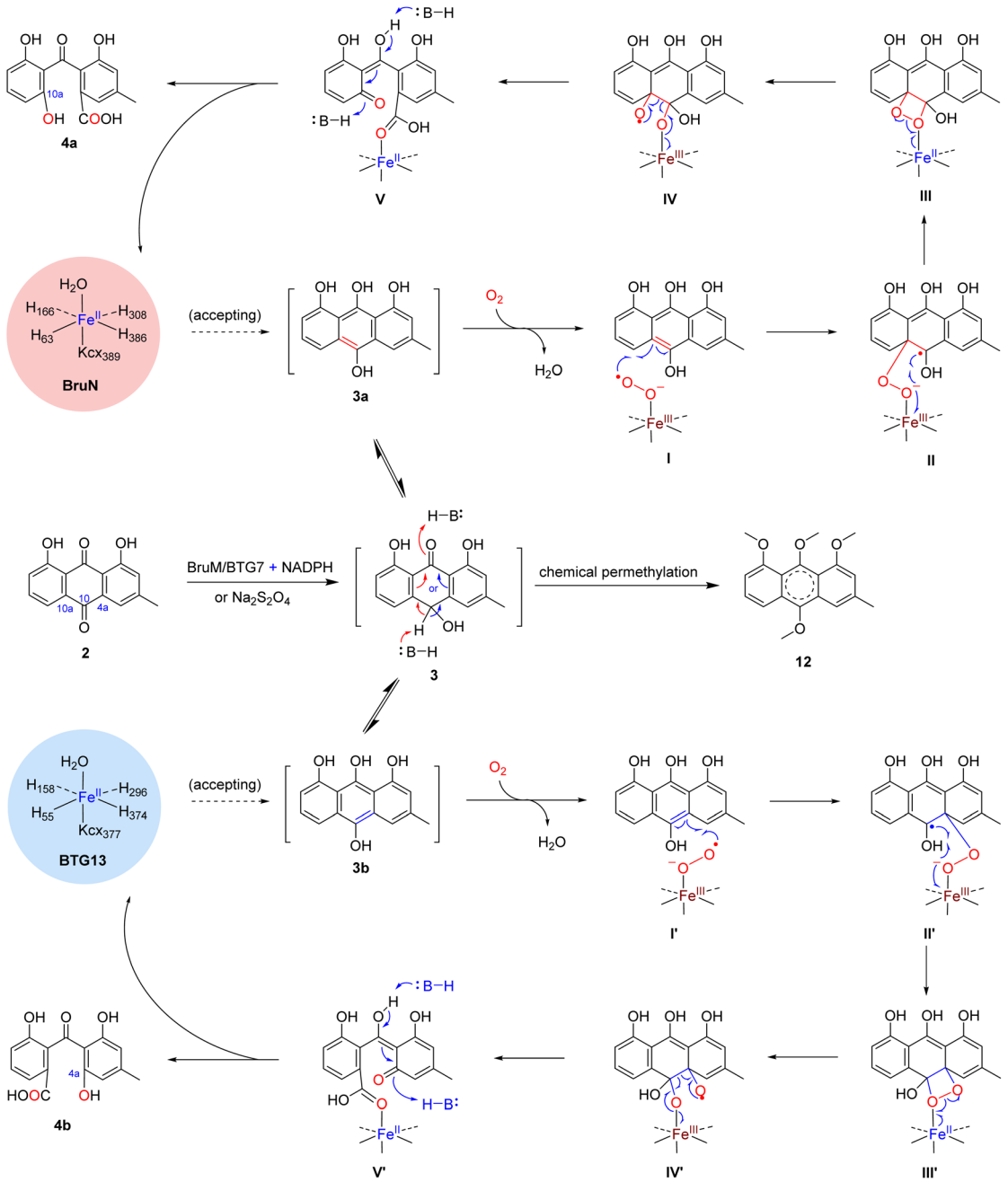

Scheme 1 Proposed catalytic mechanism underlying the regioselectivity difference between BruN and BTG13. After its reduction by $Na_2S_2O_4$, or by BruM (or BTG7) in the presence of NADPH, chrysophanol (**2**) was transformed into chrysophanol hydroquinone (**3**) which was cleaved by BruN and BTG13 into monodictyphenone (**4a**) and cephalanone F (**4b**) in C_{10a}- and C_{4a}-selective manners, respectively.

(Fig. 6D). For BTG13, the mutation of non-polar AA (M427) to a polar AA (asparagine) facilitated the C_{4a}-to-C_{10a} selectivity switch. Interestingly, if M427 was replaced by other non-polar AAs such as phenylalanine and proline, these BTG13 variants remained to be C_{4a}-selective. Next, we generated BTG13^{M427V} by substituting M427 with valine, but unexpectedly, this mutant shared the same regioselectivity with BTG13^{M427N} (*vide supra*). This could be due to the similarity in chain length between the valine and asparagine residues despite the difference in polarity, suggesting that the AA size also played a substantial role in re-shaping the binding pocket for their bindings with the **3a** tautomer. Generally speaking, the smaller the binding cavity is, the fewer AA residues need to be muted for re-shaping the cavity capable of recognizing and accepting one particular tautomer of **3**. We therefore compared the crystal structures to pinpoint that the substrate binding pocket of BTG13 is substantially smaller than that of BruN^{N441M} (Fig. S9‡). Such a difference could be among the key reason why the single-site mutation of BTG13 (M427N and M427V) could completely switch the regioselectivity, whereas BruN could only be muted

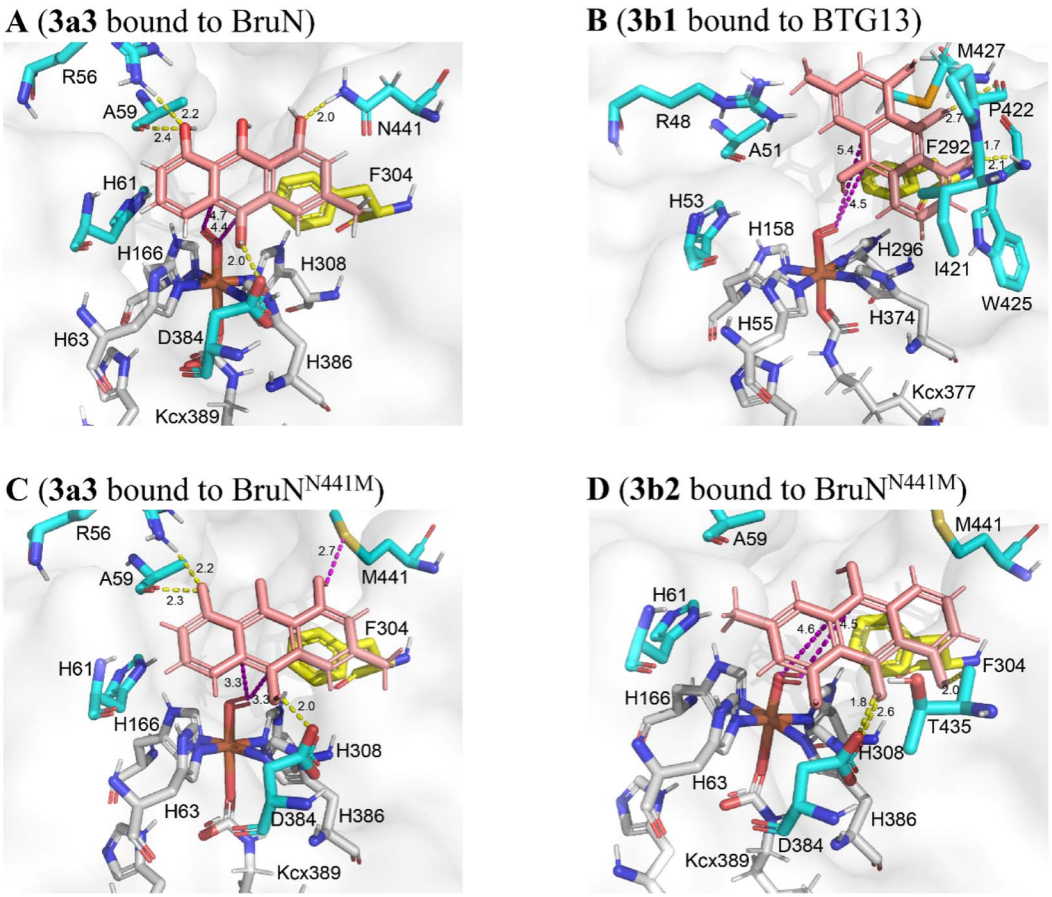

Fig. 6 Theoretical simulations of chrysophanol hydroquinone (**3**) tautomers (**3a** and **3b**) with BruN, BruN^{N441M} (PDB: 8YXS), and BTG13 (PDB: 7Y3W). (A) BruN preferred to bind **3a3**, a conformation of **3a**. (B) BTG13 interacted more effectively with **3b1**, a conformation of **3b**. (C and D) BruN^{N441M} was more interactive with **3a3** than with **3b2**, another conformation of **3b**. The magentas and yellow dashes indicated the electrostatic and hydrogen-bonding interactions, respectively. As marked in yellow, the F304 (in BruN and BruN^{N441M}) and F292 (in BTG13) residues formed the π−π stacking interactions with the **3a** and **3b** conformations. Using the AlphaFold3 program,[29] BruN$^{N441F/Q437A/V347L}$ was shown to resemble BruN^{N441M} (Fig. S9‡).

to achieve a maximal (93%) conversion rate as discerned with BruN$^{N441F/Q437A/V347L}$ (Fig. 5).

Many fungal xanthones are biosynthetically mediated by the anthraquinone-forming step,[14,18] and the carbon skeletons of end products depend crucially on the xanthone monomers and their oligomerizations.[3] To our observation, such a big family of polyketides consists largely of the homodimers of tailored xanthone monomers derived from C_{10a}- or C_{4a}-selective fissions of anthraquinone intermediates whereas the heterodimeric counterparts are much rarer (Fig. 1).[3,13] Here defined is the tunability between the C_{10a}- and C_{4a}-selectivities, which can give "non-native" cleaved anthraquinone intermediates for generating otherwise unobtainable xanthones. In this sense, the work lays the foundation for mining so far undescribed xanthones that are structurally too complex to be synthesized chemically at a reasonable or acceptable cost. Taken together, our findings are of fundamental significance in (i) facilitating more profound investigation of these families of structurally complex bioactive xanthones, and (ii) enabling the synthetic biology-based regeneration of high-value xanthones, many of which exist for unknown reasons as minor components in nature.

Conclusions

The broad involvement of regiospecific anthraquinone cleavages in the xanthone biosynthesis directed our attention to *A. brunneoviolaceus* characterized by its generation of the brunneoxanthone structures signifying the homodimerization of modified xanthone monomers forming from the C_{10a}–C_{10} bond (C_{10a}-selective) fission of anthraquinone chrysophanol (**2**).[8] Following the whole-genome sequencing of the fungus, our deletion and heterologous expression of genes led to the attribution of the C_{10a}-selectivity to the BruN (an atypical non-heme iron dioxygenase)-catalyzed fission of the 10,10a-double bond of tautomer (**3a**) of chrysophanol hydroquinone (**3**) forming from **2** under the BruM catalysis in the presence of NADPH. In correlation to our own (*vide supra*) and others' insights into the C_{4a}–C_{10} bond (C_{4a}-selective) cleavage of **2**,[14,18] we were able to disclose, and subsequently decipher the mechanism of, the tunability between the C_{10}- and C_{4a}-selectivities by a combination of directed protein evolution, theoretical simulation, chemical capture of the hydroquinone tautomer, ^{18}O chasing, and X-ray crystal structure of the BruN^{N441M} mutant. In

aggregation, the findings shed light on how to reverse or tune the regioselectively differed ring openings of anthraquinones as biosynthetic intermediates, and are thus of fundamental value for the deeper mining and/or unnatural (*e.g.*, synthetic biology-enabled) regeneration of useful polyketides *via* biotechnologies.

Data availability

The data supporting this article have been reported as part of the ESI.‡

Author contributions

X. J. L. and R. X. T. designed research and wrote paper; X. J. L., L. R. Z., and J. J. Z. performed experiments; X. J. L., X. X. M., J. P. Z., and R. X. T. analyzed data; C. Z. A. performed the computational work.

Conflicts of interest

The authors declare no competing financial interest.

Acknowledgements

This work was cofinanced by the grants from NSFC (81991524 and 22207057), the Natural Science Foundation of Jiangsu Province of China (BK20220480), and the Natural Science Foundation of the Jiangsu Higher Education Institutions of China (22KJB350002).

Notes and references

1 C. Badiali, V. Petruccelli, E. Brasili and G. Pasqua, *Plants*, 2023, **12**, 694.
2 L. X. Kong, Z. X. Deng and D. L. You, *Nat. Prod. Rep.*, 2022, **39**, 2057–2095.
3 K. M. J. de Mattos-Shipley and T. J. Simpson, *Nat. Prod. Rep.*, 2023, **40**, 174–201.
4 H. R. El-Seedi, H. M. S. Ibrahim, N. Yosri, M. A. A. Ibrahim, M. E. F. Hegazy, W. N. Setzer, Z. M. Guo, X. B. Zou, M. S. Refaey, S. E. Salem, S. G. Musharraf, A. Saeed, S. E. Salem, B. J. Xu, C. Zhao and S. A. M. Khalifa, *Curr. Med. Chem.*, 2024, **31**, 62–101.
5 M. Alam, S. Rashid, K. Fatima, M. Adnan, A. Shafie, M. S. Akhtar, A. H. Ganie, S. M. Eldin, A. Islam, I. Khan and I. Hassan, *Biomed. Pharmacother.*, 2023, **163**, 114710.
6 V. V. Vanessa and S. H. Mah, *Mini-Rev. Med. Chem.*, 2021, **21**, 2507–2529.
7 M. Gallorini, S. Carradori, D. I. S. P. Resende, L. Saso, A. Ricci, A. Palmeira, A. Cataldi, M. Pinto and E. Sousa, *Int. J. Mol. Sci.*, 2022, **23**, 13319.
8 X. J. Lv, F. Ding, Y. J. Wei and R. X. Tan, *Chin. J. Chem.*, 2021, **39**, 1580–1586.
9 J. F. Sanchez, R. Entwistle, J. H. Hung, J. Yaegashi, S. Jain, Y. M. Chiang, C. C. C. Wang and B. R. Oakley, *J. Am. Chem. Soc.*, 2011, **133**, 4010–4017.
10 S. Pornpakakul, J. Liangsakul, N. Ngamrojanavanich, S. Roengsumran, P. Sihanonth, J. Piapukiew, E. Sangvichien, S. Puthong and A. Petsom, *Arch. Pharmacal Res.*, 2006, **29**, 140–144.
11 X. X. Wei and Y. Matsuda, *Org. Lett.*, 2020, **22**, 1919–1923.
12 L. Neubauer, J. Dopstadt, H. U. Humpf and P. Tudzynski, *Fungal Biol. Biotechnol.*, 2016, **3**, 2.
13 Y. Matsuda, C. H. Gotfredsen and T. O. Larsen, *Org. Lett.*, 2018, **20**, 7197–7200.
14 X. D. Hou, H. B. Xu, Z. W. Deng, Y. J. Yan, Z. B. Yuan, X. Z. Liu, Z. P. Su, S. Yang, Y. Zhang and Y. J. Rao, *Angew. Chem., Int. Ed.*, 2022, **61**, e202208772.
15 M. T. Nielsen, J. B. Nielsen, D. C. Anyaogu, D. K. Holm, K. F. Nielsen, T. O. Larsen and U. H. Mortensen, *PLoS One*, 2013, **8**, e72871.
16 S. Sato, N. Okusa, A. Ogawa, T. Ikenoue, T. Seki and T. Tsuji, *J. Antibiot.*, 2005, **58**, 583–589.
17 K. Throckmorton, F. Y. Lim, D. P. Kontoyiannis, W. F. Zheng and N. P. Keller, *Environ. Microbiol.*, 2016, **18**, 246–259.
18 F. F. Qi, W. Zhang, Y. Y. Xue, C. Geng, X. N. Huang, J. Sun and X. F. Lu, *J. Am. Chem. Soc.*, 2021, **143**, 16326–16331.
19 Z. W. Deng, H. Su, X. D. Hou, H. B. Xu, Z. B. Yuan, X. Sheng and Y. J. Rao, *ACS Catal.*, 2024, **14**, 797–811.
20 K. Blin, S. Shaw, K. Steinke, R. Villebro, N. Ziemert, S. Y. Lee, M. H. Medema and T. Weber, *Nucleic Acids Res.*, 2019, **47**, W81–W87.
21 A. J. Szwalbe, K. Williams, Z. S. Song, K. de Mattos-Shipley, J. L. Vincent, A. M. Bailey, C. L. Willis, R. J. Cox and T. J. Simpson, *Chem. Sci.*, 2019, **10**, 233–238.
22 C. Greco, K. de Mattos-Shipley, A. M. Bailey, N. P. Mulholland, J. L. Vincent, C. L. Willis, R. J. Cox and T. J. Simpson, *Chem. Sci.*, 2019, **10**, 2930–2939.
23 Y. B. Han, W. Bai, C. X. Ding, J. Liang, S. H. Wu and R. X. Tan, *J. Am. Chem. Soc.*, 2021, **143**, 14218–14226.
24 G. Z. Dai, W. B. Han, Y. N. Mei, K. Xu, R. H. Jiao, H. M. Ge and R. X. Tan, *Proc. Natl. Acad. Sci. U. S. A.*, 2020, **117**, 1174–1180.
25 A. Krick, S. Kehraus, C. Gerhäuser, K. Klimo, M. Nieger, A. Maier, H. H. Fiebig, I. Atodiresei, G. Raabe, J. Fleischhauer and G. M. König, *J. Nat. Prod.*, 2007, **70**, 353–360.
26 Z. Z. Zhou, H. J. Zhu, L. P. Lin, X. Zhang, H. M. Ge, R. H. Jiao and R. X. Tan, *Chem. Sci.*, 2019, **20**, 73–82.
27 D. Ringe and G. A. Petsko, *Science*, 2008, **320**, 1428–1429.
28 Y. S. Wang, W. Zheng, N. Jiang, Y. X. Jin, Z. K. Meng, M. X. Sun, Y. L. Zong, T. Xu, J. P. Zhu and R. X. Tan, *Angew. Chem., Int. Ed.*, 2022, **61**, e202201321.
29 J. Abramson, J. Adler, J. Dunger, R. Evans, T. Green, A. Pritzel, O. Ronneberger, L. Willmore, A. J. Ballard, J. Bambrick, S. W. Bodenstein, D. A. Evans, C. C. Hung, M. O'Neill, D. Reiman, K. Tunyasuvunakool, Z. Wu, A. Zemgulyte, E. Arvaniti, C. Beattie, O. Bertolli, A. Bridgland, A. Cherepanov, M. Congreve, A. I. Cowen-Rivers, A. Cowie, M. Figurnov, F. B. Fuchs, H. Gladman, R. Jain, Y. A. Khan, C. M. R. Low, K. Perlin, A. Potapenko, P. Savy, S. Singh, A. Stecula, A. Thillaisundaram, C. Tong, S. Yakneen, E. D. Zhong, M. Zielinski, A. Zídek, V. Bapst,

P. Kohli, M. Jaderberg, D. Hassabis and J. M. Jumper, *Nature*, 2024, **630**, 493–500.
30 M. T. Reetz, M. Bocola, J. D. Carballeira, D. X. Zha and A. Vogel, *Angew. Chem., Int. Ed.*, 2005, **44**, 4192–4196.
31 R. M. Phelan and C. A. Townsend, *J. Am. Chem. Soc.*, 2013, **135**, 7496–7502.
32 Y. S. Wang, B. Zhang, J. P. Zhu, C. L. Yang, Y. Guo, C. L. Liu, F. Liu, H. Q. Huang, S. W. Zhao, Y. Liang, R. H. Jiao, R. X. Tan and H. M. Ge, *J. Am. Chem. Soc.*, 2018, **140**, 10909–10914.
33 D. Conradt, M. A. Schatzle, J. Haas, C. A. Townsend and M. Müller, *J. Am. Chem. Soc.*, 2015, **137**, 10867–10869.
34 M. A. Schätzle, S. M. Husain, S. Ferlaino and M. Müller, *J. Am. Chem. Soc.*, 2012, **134**, 14742–14745.
35 H. Miyabe, M. Torieda, K. Inoue, K. Tajiri, T. Kiguchi and T. Naito, *J. Org. Chem.*, 1998, **63**, 4397–4407.
36 A. Daruwalla and P. D. Kiser, *Biochim. Biophys. Acta, Mol. Cell Biol. Lipids*, 2020, **1865**, 158590.